Paper Number: **31**

Session Topic: **Fatigue of Composites**

Title: **A Cohesive Fatigue Model based on the S-N Diagram**

Authors: Carlos G. Dávila

ABSTRACT

The relationship between fatigue life and fatigue crack propagation rate is explored with a new cohesive damage model. The parameters of the model are obtained from idealizations of S-N diagrams used in engineering design. The model is based on the hypothesis that both stable tearing damage and damage due to cyclic loading are representations of a density of microcracks and, therefore, a single damage variable can describe the state of damage. This assumption implies that the quasi-static cohesive law that describes tearing is also the envelope of the fatigue damage. Fatigue damage within the cohesive envelope is assumed to accumulate at a rate that depends on the displacement jumps. The fatigue model was implemented as a UMAT subroutine for Abaqus cohesive elements by adding fatigue damage accumulation to a cohesive model based on the Turon quasi-static cohesive law. The analyses were conducted using a simplified cyclic loading procedure in which the maximum applied load is kept constant and the computational expense of cycling the load is avoided. The predicted propagation rates for a double cantilever beam (DCB) specimen were compared to experimental results for IM7/8552 graphite/epoxy tape.

INTRODUCTION

Engineering calculations of fatigue life are usually performed using stress-life diagrams, called S-N curves [1]. These curves represent the number of cycles that a material can sustain at a given stress level before failure. The data to generate these curves is obtained by cycling smooth or notched specimens until failure. The S-N curves of many materials are simple and can be approximated by straight lines in a log-log plot. In addition, analysis techniques have been developed to account for the

---

Carlos G. Dávila, NASA Langley Research Center, Structural Mechanics and Concepts Branch, MS 190, Hampton, VA 23681, USA

effect of the ratio of the minimum to the maximum stress on the S-N curves. Since these calculations essentially depend on the knowledge of the stress state, predicting fatigue life with S-N diagrams does not require specialized computational tools.

On the other hand, predicting fatigue crack propagation is significantly more difficult. First, fracture mechanics tools are required because the rate of crack propagation, defined as a crack extension, da, per incremental number of cycles, dN, is a function of the energy release rate (ERR), G. The rate of crack propagation in fatigue is often described with the Paris law:

$$\frac{\mathrm{d}a}{\mathrm{d}N} = C\left(G\right)^m \tag{1}$$

where G is the ERR and C and m are material constants that vary with stress ratio and mode mixity. When Eq. 1 is plotted on log-log axes, it appears as a straight line relating the propagation rate da /dN to G.

Cohesive element formulations to predict the nucleation and propagation of cracks in composite structures subjected to cyclic fatigue have been the subject of intense development for almost two decades. The main difficulty in the development of a cohesive fatigue damage model consists in linking the rate of change of the damage variable, d, to the crack propagation rate [2]. Turon's fatigue model [3] proposes linking the two as follows:

$$\frac{\mathrm{d}d}{\mathrm{d}N} = \frac{1}{l_{pz}} \frac{\left(\Delta^f\left(1-d\right)+\Delta^c d\right)^2}{\Delta^f \Delta^c} \frac{\mathrm{d}a}{\mathrm{d}N} \tag{2}$$

where $\mathrm{d}d/\mathrm{d}N$ is the rate of change of the damage variable, l_{pz} is the length of the process zone, i.e., the zone where the damage is partially developed, Δ^f is the maximum displacement jump of the cohesive law, Δ^c is the displacement jump for damage initiation, and $\mathrm{d}a/\mathrm{d}N$ is the propagation rate expressed by the Paris law. The damage variable is defined such that (1-d) is the ratio of the damaged stiffness over the initial stiffness of the cohesive law. The length of the process zone appears in this expression because the damage variable at any particular point along the path of the crack must gradually increase from zero to one as the entire process zone traverses that point. Therefore, for a given propagation rate, $\mathrm{d}a/\mathrm{d}N$, the longer the l_{pz}, the larger number of cycles for the damage variable to reach one. Since the fatigue damage rate at a material point depends on the damage state at other locations, the model described by Eq. 2 is nonlocal.

A number of local damage models that attempt to predict fatigue crack propagation without the Paris law have also been proposed. In fact, most of the earlier cohesive fatigue models were local formulations. For instance, Nojavan [4] proposed a local model for mixed-mode delamination in which an S-N response is used to initiate damage. After initiation, an empirical expression based on the displacement jumps is used to accumulate damage. As in all of the local models presented in the literature, the coefficients of the damage model are determined by trial and error by comparing the predictions with experimental results. The review by Bak et al. [5] of experimental observations also provides an insightful classification of various fatigue models and their predictive capabilities.

In the proposed model, fatigue damage inside the cohesive law envelope is assumed to accumulate according to a simple two-parameter law at a rate that depends on the displacement jump. Unlike other local models of this type, the two parameters of the damage law are solved using an idealization of S-N diagrams commonly used in engineering design.

The present paper is organized as follows. In the following section, an idealization of S-N diagrams based on estimates of the endurance limit is presented. Engineering approaches are used to account for the stress ratio R. A two-parameter damage law is presented next. It is shown that the two parameters are functions of the stress ratio, and that they can be obtained from the corresponding S-N diagrams. Then, the ability of the model to predict crack propagation rates is evaluated by examining the results of a double cantilever beam (DCB) test.

A COHESIVE FATIGUE MODEL BASED ON AN ASSUMED S-N DIAGRAM

The S-N curve is one of the simplest descriptions of the failure of a material as a function of the applied cyclic load. For example, the transverse tension fatigue lives of unidirectional IM7/8552 graphite/epoxy flexure specimens oriented at 90° to the longitudinal axis are plotted in Fig. 1 [6]. The specimens were subjected to a stress ratio $R = \sigma^{min}/\sigma^{max} = 0.1$. Despite the fact that the experimental results depend on the volume of the specimen, the mode of testing, and the degree of surface polishing, the fatigue data, when normalized by the static strength, σ_c, can be approximated by a straight line. (Note: subscripts are used to identify properties of the material or model, as opposed to operating variables, identified with superscripts).

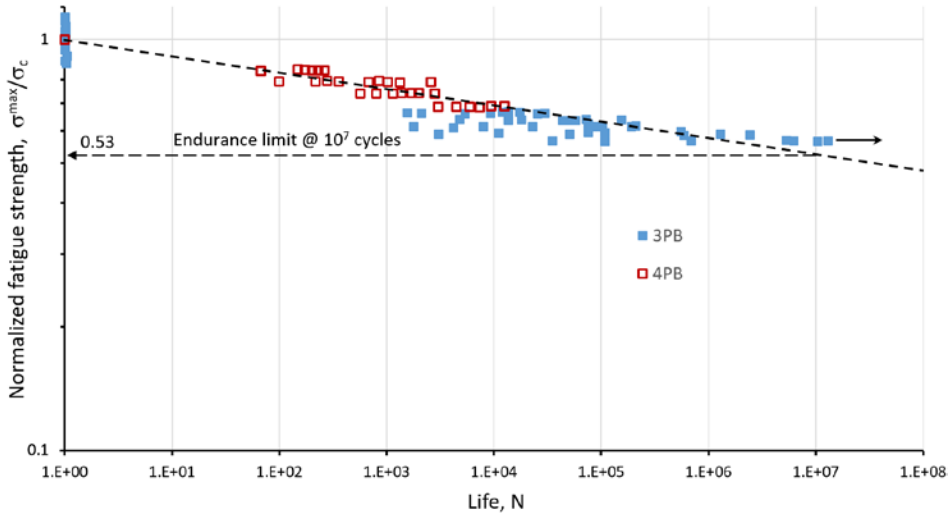

Figure 1. S-N curve for matrix failure of IM7/8552 at $R = 0.1$ [6].

For some materials, including steels, the S-N diagram requires three lines. The first of these lines represents the low-cycle or ductile response of a material when it is subjected to high cyclic stresses. The second line represents the high-cycle response. The last line is horizontal, which represents the endurance limit cutoff below which the lives of the specimens are not affected by fatigue damage. Fleck [7] defines the

endurance limit, σ_e, as the stress amplitude that a smooth unnotched sample will sustain without fracture for 10^7 cycles. The results in Fig. 1 suggest that a single line fits the low-cycle and high cycle portions of the graph, so there is no need to distinguish between the two when considering the transverse tensile loading of IM7/8552. However, the arrow next to one of the data points in Fig. 1 indicates that a runout occurred for that point. Due to the absence of data and for simplicity, no endurance cutoff was considered in the present work.

Estimating the Endurance Limit

A particularly appealing aspect of the straight line approximation of an S-N curve is that the entire curve is described by a single value: the endurance limit [1]. In addition, the endurance limit can be estimated quite easily from the material strength. As early as the 19th century, Goodman [8] observed that the endurance limit of steels subjected to fully reversed loading is approximately equal to 1/3 of the yield strength. Fleck [7] performed fatigue tests on materials including polymer foams, elastomers, woods, polymers, composites, metallic alloys, and engineering ceramics and confirmed that the 1/3 ratio is valid for a wide range of materials. This observation is evident in Fig. 2, which was generated using the 3078 materials in the complete CES Selector material library [9].

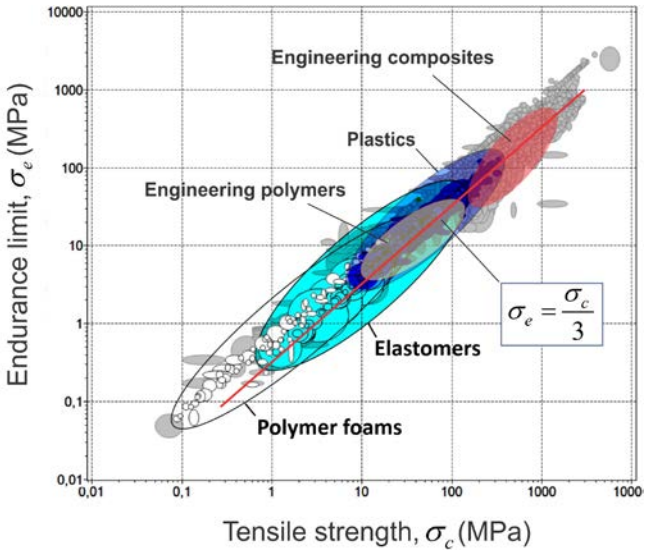

Figure 2. Endurance limit vs. tensile strength [chart courtesy of Stéphane Gorsse, ICMCB-CNRS and Bordeaux INP, France; property chart generated with the CES Edupack, Granta Design].

Effect of stress ratio *R* on Endurance Limit

The endurance limit is usually measured using a rotating-beam specimen that subjects the material sample to a full reversal of the load ($R = -1$). A procedure to estimate the endurance limit for other values of the stress ratio is as follows. Consider the cyclic loading illustrated in Fig. 3, where R is greater than zero.

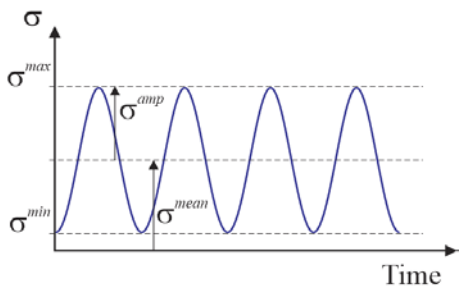

Figure 3. Cyclic loading.

The stress amplitude, σ^{amp}, and the mean stress, σ^{mean}, can be written in terms of the stress ratio R as:

$$\sigma^{amp} = \sigma^{\max}\frac{1-R}{2} \qquad \sigma^{mean} = \sigma^{\max}\frac{1+R}{2} \tag{3}$$

The Goodman diagram [8], a plot of alternating versus mean stress, is a design tool that represents the locus of stress states corresponding to a runout stress or a given number of cycles to failure, for example, 10^7. The Goodman model postulates a straight line connecting the endurance limit, σ_e, on the y-axis with the ultimate stress, σ_c, on the x-axis, as shown in Fig. 4. The allowable stress amplitude, σ^{amp}, is then defined as a function of mean stress, σ^{mean}, as

$$\sigma^{amp} = \sigma_e\left(1-\frac{\sigma^{mean}}{\sigma_c}\right) \tag{4}$$

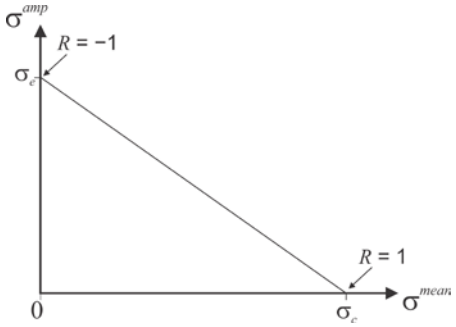

Figure 4. Goodman diagram.

The endurance $\sigma_{eR} = \sigma^{\max}$ is defined as the maximum stress for a stress ratio R that satisfies the Goodman relation. The endurance is then obtained by substituting Eq. 3 into Eq. 4:

$$\sigma_{eR}\left(\frac{1-R}{2}+\frac{1-R}{2}\frac{\sigma_e}{\sigma_c}\right) = \sigma_e \tag{5}$$

Substituting Fleck's [7] expression, $\sigma_e = \frac{1}{3}\sigma_c$, into Eq. 5 gives the endurance as a function of the stress ratio R:

$$\sigma_{eR} = \frac{\sigma_c}{2 - R} \tag{6}$$

The values of the endurance calculated from Eq. 6 are listed in Table I for several typical values of *R*. It can be observed that the endurance for $R = 0.1$ is $\sigma_{eR} = 0.53\,\sigma_c$. This value is consistent with the endurance used to fit the data in Fig. 1.

In summary, the present model relies on Eq. 6 and the assumption of linearity of an S-N log-log plot to establish the S-N diagram for any material and stress ratio.

TABLE I. ENDURANCE AS A FUNCTION OF STRESS RATIO *R*.

R	σ_{eR}
-1	$\frac{1}{3}\sigma_c \ (=\sigma_e)$
0	$\frac{1}{2}\sigma_c$
0.1	$0.53\ \sigma_c$
0.5	$\frac{2}{3}\sigma_c$

Cohesive Fatigue Damage Model

Consider an unnotched bar subjected to tensile cyclic loads, as shown in Fig. 5. A fatigue crack is assumed to occur at the center of the bar. The two-piece failure of the bar can be assumed to occur after a number of cycles, which depends on the maximum applied stress load, σ^{max}, and the life specified by the S-N diagram.

Figure 5. Unnotched bar subjected to cyclic loads.

A cohesive fatigue law is illustrated in Fig. 6a. The outline of the cohesive law is composed of an elastic range *O-E*, followed by the "tearing" curve, *E-T*. Since any point outside of the cohesive outline corresponds to a failed material state, the outline represents the envelope of the damage process.

When the maximum applied stress, σ^{max}, is less than the strength σ^c, the material damages in fatigue without ever traversing the portion *A-E-F* of the cohesive law. Instead, at any point *P* (Fig. 6b) damage *d* accumulates with the number of cycles. Consequently, the maximum displacement jump λ increases gradually from point *A* to point *F*. At point *F*, σ^{max} exceeds the load-carrying ability of the material defined by the tearing portion *E-T* of the cohesive envelope and unstable failure ensues.

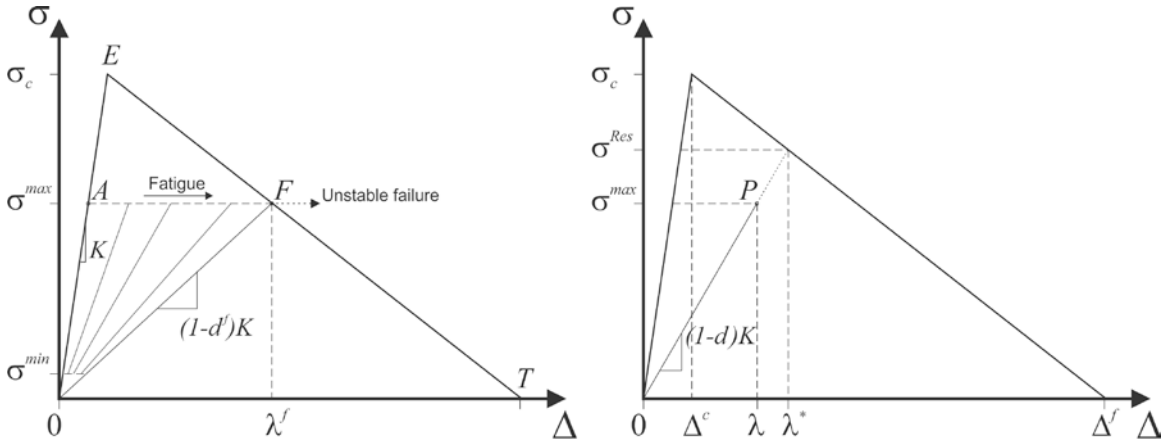

a) Description of fatigue under σ^{max} = constant. b) Definition of displacement jumps in fatigue.

Figure 6. Cohesive law with fatigue damage – definition of failure envelope and variables.

The evolution of fatigue damage is a function of the applied cyclic load and the damage state. The following two-parameter heuristic fatigue damage model is proposed:

$$\frac{\mathrm{d}D}{\mathrm{d}N} = \left(D+\gamma\right)\left(\frac{\lambda}{\lambda^*}\right)^{\beta} \tag{7}$$

where the damage norm D is defined as [3]:

$$D = \frac{\lambda^* - \Delta^c}{\Delta^f - \Delta^c} \tag{8}$$

and where the relative displacement jump at any point P is

$$\frac{\lambda}{\lambda^*} = \frac{\sigma^{\max}}{\left(1-D\right)\sigma_c} \tag{9}$$

The damage norm D can be interpreted as the ratio of the energy dissipated during the damage process over the critical energy release rate. Consequently, D is also the ratio of the damaged area over the area associated with the local discretization [3]. This norm is a linear function of the displacement jump λ^* and it is independent of the penalty stiffness. The loss of stiffness (1-d) of the cohesive law is related to D as follows:

$$1-d = \frac{\lambda^* - \Delta^f D}{\lambda^*} \tag{10}$$

For the one-dimensional constant-amplitude problem considered in Fig. 5, the total number of cycles from A to unstable failure (point F in Fig. 6a) can be calculated by integrating Eq. 7 for the range of damage $D = 0$ to D^F. The result is:

$$N^f = \left(\frac{\sigma_c}{\sigma^{\max}} \right)^{\beta} \int_0^{D^F} \frac{(1-D)^{-\beta}}{D+\gamma} \, \mathrm{d}D \tag{11}$$

where D^F is the damage at point F (Fig. 6a):

$$D^F = 1 - \frac{\sigma^{\max}}{\sigma_c} \tag{12}$$

Eq. 11 represents the number of cycles to failure under a constant amplitude cyclic load in terms of the maximum stress ratio, $\sigma^{\max} / \sigma_c$. The pair of coefficients β, γ that defines the damage model in Eq. 7 can be determined by fitting the results of Eq. 11 onto an S-N curve. The next section outlines the procedure to determine these coefficients.

Determination of Coefficients β and γ for IM7/8552

The coefficients $\beta(R)$ and $\gamma(R)$ are functions of the stress ratio R. They are calculated by fitting the curves obtained by the integral in Eq. 11 to the material S-N curve for the corresponding stress ratio. The fitting is achieved by specifying two anchor points. The first point corresponds to a high maximum stress ratio that represents the end of the low-cycle fatigue portion of the S-N curve. In ductile materials, the range between the first cycle and the first anchor point can be significant. In the present study, this point is arbitrarily set equal to two cycles, which translates into a short ductile range that appears to fit data shown in Fig. 1 well. The second anchor point is set by the endurance limit, which is calculated with Eq. 6 and reported in Table I. The calculation of the constants β and γ involves the solution of a nonlinear system of two equations for the range of stress ratios.

The coefficients β and γ for several typical stress ratios are reported in Table II, and the corresponding S-N curves are shown in Fig. 7. The curve for R = 0.1 is darker than those for other stress ratios to highlight the fact that the test data, also shown, corresponds to this stress ratio.

Finally, it is important to emphasize that the coefficients (β ; γ) can be determined by fitting the results of Eq. 11 to experimental data. However, in the present work, they are calculated based on the endurance limits estimated with the use of Eq. 6.

TABLE II. COEFFICIENTS (β ; γ) FOR SEVERAL VALUES OF THE STRESS RATIO.

R	β	γ
-1	13.611	0.001911
0	21.842	0.002142
0.1	23.649	0.002194
0.5	38.033	0.002643

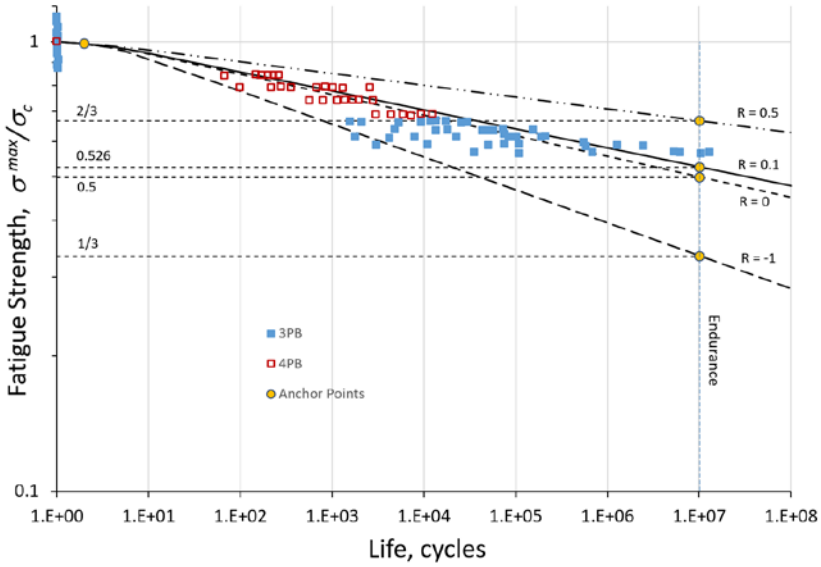

Figure 7. S-N curves for different stress ratios obtained using Eq. 11 and the coefficients in Table II. The test data shown by the symbols is for R = 0.1.

Predicting Crack Propagation with Simplified Cyclic Loading (SCL)

The cohesive fatigue model proposed in Eq. 7 and the determination of the coefficients β and γ described in the previous section are based on the assumption that damage, i.e., a measure of microcrack density and loss of stiffness at a material point, characterizes simultaneously a degradation of the material by fatigue or by tearing. In other words, the model assumes that both states of damage evolve together such that a reduction in remaining life is always accompanied with a degradation of the tearing resistance and vice-versa. This assumption ensures that the envelope of the cohesive law is valid for tearing, for fatigue, or for any combination of the two so that a single variable, d, is sufficient to track the effects of all aspects of the past loading history at a material point. Therefore, the model is notionally capable of accounting for damage accumulation anywhere within the cohesive envelope. Although the model coefficients are determined from the constant maximum stress conditions of an S-N diagram, the model can capture the fatigue damage accumulation along any loading path.

The fatigue damage model was implemented in a finite element framework as a cohesive constitutive model and solved within a simplified cyclic loading (SCL) procedure that avoids the computational expense of having to cycle the applied load. In SCL, the maximum load is held constant. For simplicity, the frequency of cyclic loading is 1 Hz, so that the analysis pseudo-time represents the number of cycles, as illustrated in Fig. 8. The effect of cycling on fatigue damage is represented by the stress ratio R within the constitutive damage model. The analysis is conducted in two steps. The first step from 0 to 1 introduces the applied load (force or displacement). No fatigue damage is allowed in the first step. During the second step, the applied load is held constant but the solution is recalculated to account for the internal load redistribution that occurs with fatigue and tearing damage accumulation.

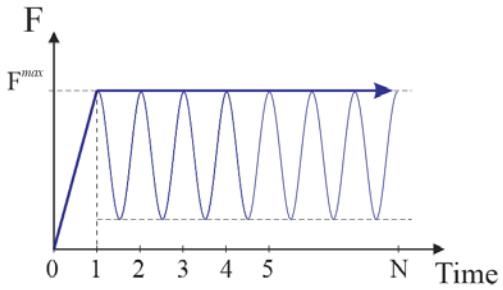

Figure 8. SCL procedure: the load is held constant during the analysis while the effects of loading amplitude, stress ratio, cycle count, and damage accumulation are processed within the constitutive model.

A user-written UMAT subroutine for Abaqus cohesive elements was developed. UMAT subroutines are called by the Abaqus implicit solver at every integration point, at every equilibrium iteration of every time increment. The subroutine receives the current damage state, the displacement jump, and the analysis time increment. The output of the subroutine is the damage state. A UMAT for fatigue damage was written by modifying a UMAT of Turon's quasi-static cohesive model [10]. Implementation of the fatigue model within the quasi-static cohesive UMAT only required adding the calculation of the fatigue damage.

VALIDATION: CRACK PROPAGATION IN MODE I AND MIXED MODE

Analysis of Double Cantilever Beam Specimen

The double cantilevered beam (DCB) specimen is a standardized test method for determining the onset of delamination propagation for mode I loading [11]. The DCB specimen has also been used for determining the delamination growth rate in fatigue. The results of an extensive characterization of delamination onset and growth under Mode I fatigue loading of IM7/8552 graphite/epoxy unidirectional tape specimens by Murri [12] were used in the present study to evaluate the ability of the proposed model to predict delamination propagation rates.

The DCB specimens tested by Murri were manufactured with 24 plies of IM7/8552 unidirectional tape with a thin Teflon film at the mid-plane at one end to induce an initial delamination. The specimens were nominally 178-mm long and 25.4-mm wide. The configuration of the test specimen is defined by the nominal dimensions reported in Table III.

TABLE III. DIMENSIONS OF DCB SPECIMEN IN MM.

a_0	b	h
50.8	25.4	2.25

The parametric model of a DCB specimen shown in Fig. 9 was constructed in Abaqus/Standard [13]. The model parameters can be used to change the dimensions of the specimen and the number of elements in each of the regions of the model. For computational efficiency, the width of the model is 1 mm and the reaction force is scaled by the width b = 25.4 mm of the specimen. The propagation zone length varied

between 5 mm and 15 mm, depending on the length of crack propagation that was needed. To ensure accurate trends in the crack propagation rates, the element edge length in the propagation zone of the model is 0.04 mm. A mesh convergence study indicated that an element size up to 0.1 mm is sufficient to predict crack length as a function of cycles, but the propagation rate becomes noisy. Three layers of SC8R continuum shell elements were used through the thickness of each arm, and three elements were used across the width. The material properties used in the analysis are provided in Table IV, and were generated within the scope of the NASA Advanced Composites Project (ACP) [14].

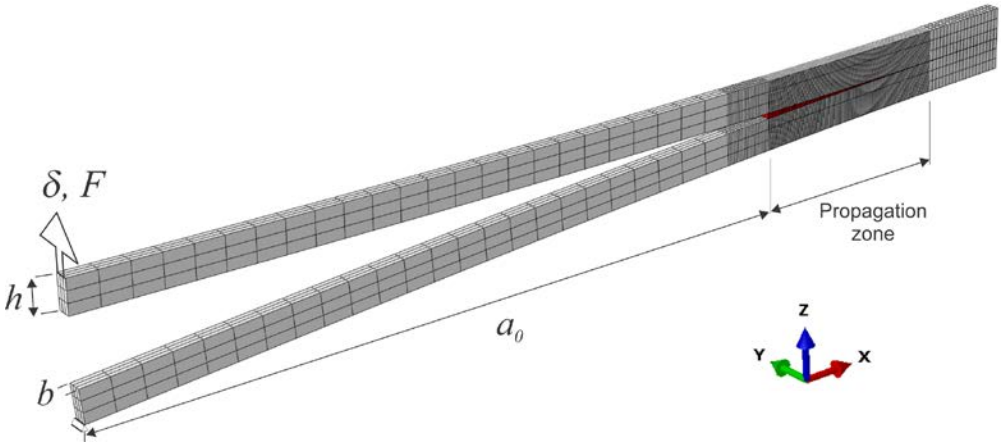

Figure 9. Finite element model of a 1-mm-wide strip of a DCB specimen.

TABLE IV. MATERIAL PROPERTIES OF IM7/8552 [14].

$E_{11\,(avg\ T/C)}$	146,671.	MPa
$E_{22}=E_{33}$	8703.	MPa
$G_{12}=G_{13}$	5164.	MPa
G_{23}	3001.	MPa
G_{Ic}	0.240	N-mm/mm^2
G_{IIc}	0.739	N-mm/mm^2
σ_c	80.1	MPa
τ_c	97.6	MPa
η	2.1	

To simulate the experimental procedure, which was conducted under displacement control, the model was loaded with a constant applied displacement, δ, and the reaction force, F, was recorded as a function of the number of cycles.

Predicting Paris Law Propagation Rate

The crack length, a, can be obtained by direct examination of the finite element model at repeated cycle increments, although such post-processing can be tedious.

Alternatively, the crack length can be calculated from the compliance $C=\delta/F$ of the model using a closed form expression derived by the corrected beam theory. The ERR during the simulation varies as a function of the reaction force F and the crack length. Details on the procedure to extract the crack length and ERR from the compliance can be found in Dávila [15].

Analyses were performed with applied displacements δ_{max} = 1.48 mm, 1.7 mm, 1.92 mm, and 2.25 mm. At the start of the analyses, these displacements correspond to G/G_{Ic} ratios of 0.3, 0.4, 0.5, and 0.69, respectively. As the cracks propagate, these ratios become smaller. The rates of propagation were obtained by calculating $\Delta a/\Delta N$ from the crack lengths obtained at a number of time increments. The analysis results and the corresponding experimental values are shown in Fig. 10. The arrows indicate the direction of progression, from the start towards the end of the simulations. The blue circular symbols shown on the predicted curves in Fig. 10 correspond to a 5% increase in specimen compliance compared to the compliance at the start of the simulation. This change occurs after 0.9 mm of delamination propagation. This point is sometimes referred to as the 5% onset [16].

The predicted propagation rates start high and then quickly reduce to a rate that falls onto the straight line of a Paris law. The initial transient response is the result of the formation of a process zone, which starts with the tearing damage caused by the first loading cycle, and then grows under the cyclic loading to a stable size. The band of red elements in Fig. 11a correspond to the process zone. The elements to the left of the process zone are completely damaged, and those to the right are intact. The crack extension as a function of the number of cycles is reported in Fig. 11b. The points correspond to lengths of propagation measured from the analysis results in Fig. 11a, and the curve was obtained using the compliance solution. Both methods provide similar results, but the compliance method is much easier to generate.

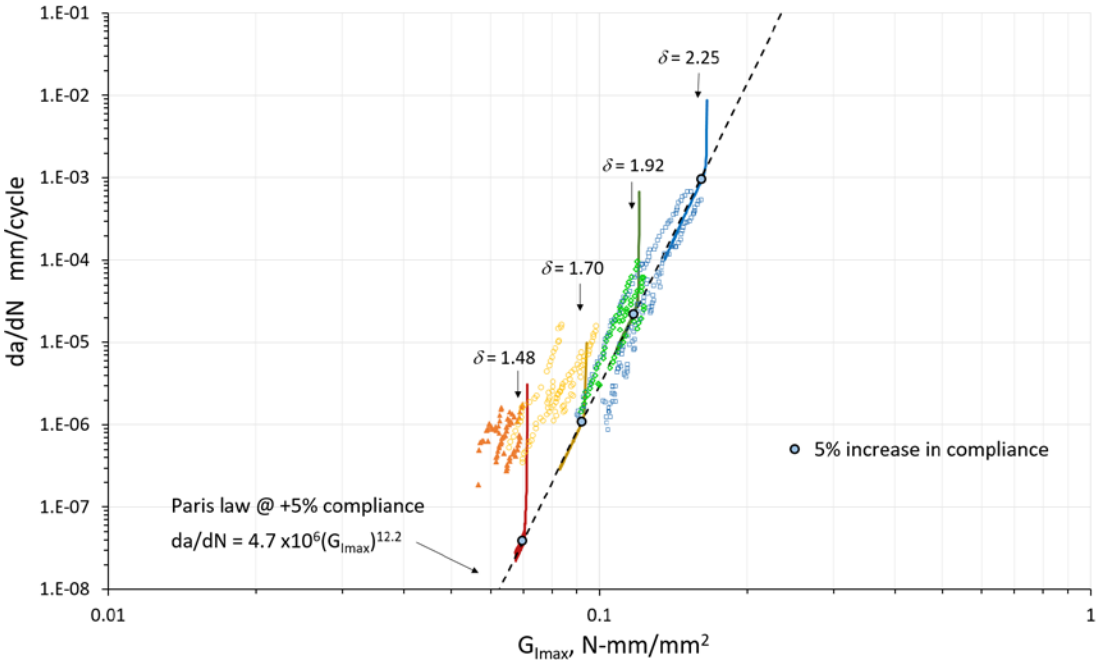

Figure 10. Comparison of measured and predicted delamination growth rates in a DCB specimen for different values of the applied displacement.

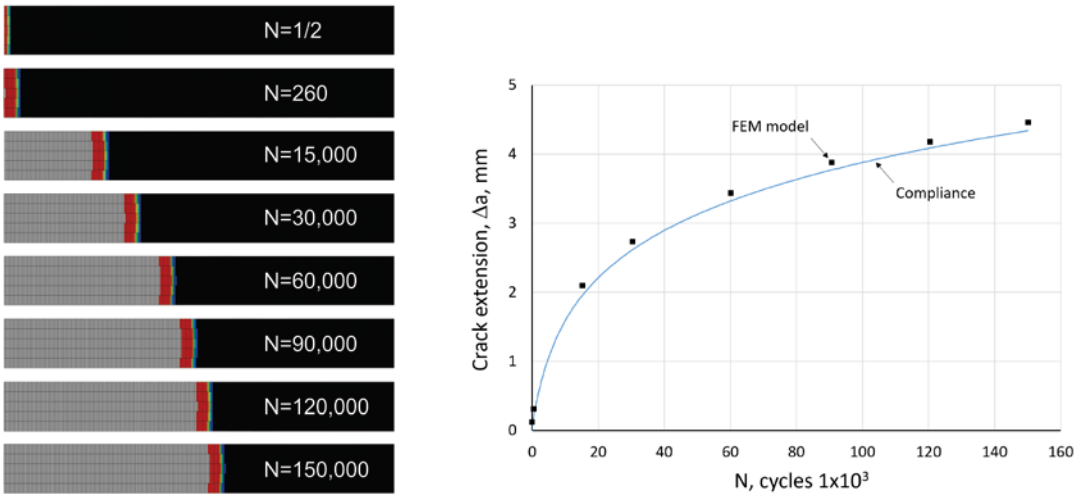

a) Detail of propagation of process zone. b) Crack extension as a function of cycle count.

Figure 11. Crack propagation in DCB specimen with applied displacement δ_{max} = 1.92 mm.

At steady-state propagation, the l_{pz} is observed to be approximately 0.3 mm, and l_{pz} remains constant during propagation despite the fact that the ERR and the corresponding crack propagation rate decrease with crack length. In fact, the length of the process zone appears to be independent of the applied cyclic load and nearly identical to the 0.35 mm that forms by quasi-static tearing.

The results of the analyses for different R ratios (see Ref. [15]) indicate that there is a relationship between the stress ratio R and the following: the endurance limit (Eq. 6), the exponent β of the damage model (Eq. 7), and the slope m of the Paris law. The relationship between β and m, which ties the S-N diagram to the Paris law, appears to be linear.

The results also indicate that the coefficient C of the Paris law is a function of factors that do not affect m, including the strength σ_c and the critical energy release G_c. To illustrate the sensitivity of the predicted propagation rate on these two material properties, two analyses of the DCB specimen were performed in which σ_c and G_c were increased by 50% over their nominal values. In the first analysis, the strength was increased from 80 MPa to 120 MPa, while all other properties remained at their nominal values. In the second analysis, G_c was increased from 0.24 N-mm/mm^2 to 0.36 N-mm/mm^2. The results of the analyses are compared to the nominal results in Fig. 12. Paris lines were fit through the predicted propagation rates, and the coefficients C of the lines were used to calculate the relative propagation rates. The predicted crack propagation rate for a 50% increase in strength is 2.6 times slower than predicted with the nominal strength value, and the predicted rate for a 50% increase in G_c is 94 times slower than predicted with the nominal G_c value.

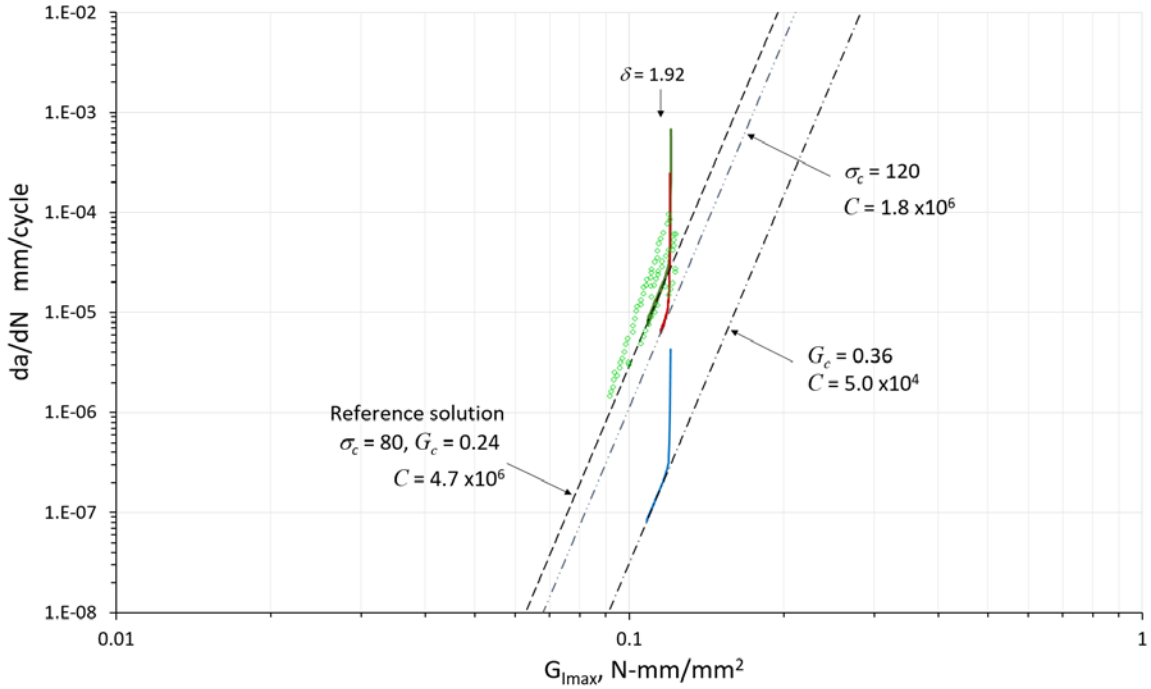

Figure 12. Predicted fatigue crack propagation rate for DCB specimen with nominal properties compared to predicted fatigue crack propagation rate with either strength or critical ERR increased by 50%.

SUMMARY AND DISCUSSION

The relationships between the material properties that describe tearing (G_c, σ_c), those that describe fatigue life (S-N), and those that describe crack propagation rates (Paris law) are explored using a new cohesive fatigue damage model. The model relies on the former two characterizations (tearing and life) to predict the latter two (onset and Paris law). The proposed fatigue model assumes that a single variable is sufficient to represent the historical effects of load cycles on damage at a material point, regardless of whether the damage was caused by tearing or by fatigue. With this assumption, the quasi-static cohesive law becomes the envelope of the fatigue law. Fatigue damage inside the envelope accumulates at a rate that depends on the displacement jumps. The damage model relies on the simplicity of typical S-N diagrams and the fact that the endurance limit can often be estimated from the quasi-static strength without performing any fatigue tests. The two parameters required by the model, β and γ, are extracted from the quasi-static properties and the S-N idealizations.

The fatigue cohesive model proposed is capable of predicting interfacial failure in unnotched problems where life and S-N diagrams dominates the physics of the problem, as well as the crack propagation rate, where the Paris law is typically used. The fatigue model was implemented as a user-written subroutine UMAT for Abaqus using Turon's cohesive law. The predictive capability of the fatigue model was evaluated by comparing predicted crack propagation rates in DCB specimens composed of IM7/8552 graphite/epoxy material with experimental data.

REFERENCES

1. Shigley, J. E., and Mitchell, L. D., *Mechanical Engineering Design*, McGraw-Hill Book Company, New York, NY, 1983.
2. Bak, B. L. V., Turon, A., Lindgaard, E., and Lund, E., "A Benchmark Study of Simulation Methods for High-Cycle Fatigue-Driven Delamination Based on Cohesive Zone Models," *Composite Structures*, Vol. 164, 2017, pp. 198-206.
3. Turon, A., Costa, J., Camanho, P. P., and Dávila, C. G., "Simulation of Delamination in Composites under High-Cycle Fatigue," *Composites Part A: Applied Science and Manufacturing*, Vol. 38, No. 11, 2007, pp. 2270-2282.
4. Nojavan, S., Schesser, D., and Yang, Q. D., "An in Situ Fatigue-Czm for Unified Crack Initiation and Propagation in Composites under Cyclic Loading," *Composite Structures*, Vol. 146, No. Supplement C, 2016, pp. 34-49.
5. Bak, B. L., Sarrado, C., Turon, A., and Costa, J., "Delamination under Fatigue Loads in Composite Laminates: A Review on the Observed Phenomenology and Computational Methods," *Applied Mechanics Reviews*, Vol. 66, No. 6, 2014, p. 060803.
6. O'Brien, T. K., Chawan, A. D., Krueger, R., and Paris, I. L., "Transverse Tension Fatigue Life Characterization through Flexure Testing of Composite Materials," *International Journal of Fatigue*, Vol. 24, No. 2-4, 2002, pp. 127-145.
7. Fleck, N. A., Kang, K. J., and Ashby, M. F., "Overview No. 112: The Cyclic Properties of Engineering Materials," *Acta Metallurgica et Materialia*, Vol. 42, No. 2, 1994, pp. 365-381.
8. Goodman, J., *Mechanics Applied to Engineering*, Longmans, Green and Co., London, UK, 1899.
9. *CES Selector Software*, Granta Design Limited, Cambridge, UK, 2017.
10. Turon, A., González, E. V., Sarrado, C., Guillamet, G., and Maimí, P., "Accurate Simulation of Delamination under Mixed-Mode Loading Using a Cohesive Model with a Mode-Dependent Penalty Stiffness," *Composite Structures*, Vol. 184, No. Supplement C, 2018, pp. 506-511.
11. ASTM D5528-01, "Standard Test Method for Mode I Interlaminar Fracture Toughness of Unidirectional Fiber-Reinforced Polymer Matrix Composites," *Annual Book of ASTM Standards*, American Society for Testing and Materials, West Conshohocken, PA, 2002.
12. Murri, G. B., "Evaluation of Delamination Onset and Growth Characterization Methods under Mode I Fatigue Loading," Technical Report NASA/TM–2013-217966, Hampton, VA, Feb. 2013.
13. Dassault Systèmes, *Abaqus® 2017 Documentation*, Simulia Corp., Providence, RI, USA, 2017.
14. Wanthal, S., Schaefer, J., Justusson, B., Hyder, I., Engelstad, S., and Rose, C. A., "Verification and Validation Process for Progressive Damage and Failure Analysis Methods in the NASA Advanced Composites Consortium," American Society for Composites Technical Conference, Purdue University, West Lafayette, IN, 23-25 Oct. 2017.
15. Dávila, C. G., "From S-N to the Paris Law with a New Mixed-Mode Cohesive Fatigue Model," Technical Report NASA/TM–2018 (in review), Hampton, VA, May 2018.
16. ASTM D 6115 – 97, "Standard Test Method for Mode I Fatigue Delamination Growth Onset of Unidirectional Fiber-Reinforced Polymer Matrix Composites," *Annual Book of ASTM Standards*, American Society for Testing and Materials, West Conshohocken, PA, 2002.